

Study of Laminar Forced Convection Heat Transfer for Dimpled Heat Sinks

Doseo Park,* Carlos Silva,* Egidio (Ed) Marotta,[†] and Leroy (Skip) Fletcher[‡]
Texas A&M University, College Station, Texas, 77843-3123

DOI: 10.2514/1.33497

An investigation was conducted to determine whether dimpled surfaces could improve the heat transfer in a heat sink under laminar airflows. This was accomplished by performing experimental and numerical investigations using two different dimple geometries: 1) circular (spherical) and 2) oval (elliptical or trenched) dimples. Dimples with a relative pitch of $S/D = 1.21$ and relative depth of $\delta/D = 0.2$ (e.g., circular dimples) were machined on both sides of copper plates, then placed into a channel with airflow impinging over the leading edge of the plate. For oval dimples, similar ratios with the same total depth and circular edge-to-edge distance as the circular dimples were used. For those configurations the average heat transfer coefficient and Nusselt number ratio were determined experimentally. Heat transfer enhancements up to a 6% relative to a flat plate were consistently observed for Reynolds number (based on channel height) in the range of 500 to 1650 on both circular and oval dimples. Additionally, pressure drop, thermal performance, and flow characteristic were simulated numerically. The heat transfer coefficients in our numerical experiment were close to those of the experimental investigation for Reynolds number up to 750. The pressure drop over the dimpled plates was either equivalent to or less than that of the flat plate with no dimples.

Nomenclature

A_S	=	surface area, m ²
C_p	=	specific heat, K
D	=	dimple print diameter, m
f	=	friction factor
f_0	=	friction factor of a flat plate
H	=	channel height, m
h	=	average heat transfer coefficient, Wm ⁻² K ⁻¹
I	=	current supplied to the heater, A
K	=	thermal conductivity, Wm ⁻¹ K ⁻¹
m	=	mass flow rate of air, kg s ⁻¹
Nu	=	overall average Nusselt number
Nu_0	=	overall average Nusselt number of a flat plate
Q_{loss}	=	extraneous heat loss, W
Q_{net}	=	net heat transfer rate, W
Q_{total}	=	heat transfer from heater, W
S	=	dimple pitch, m
T_b	=	mean bulk temperature, K
$T_{b,\text{inlet}}$	=	inlet bulk temperature, K
$T_{b,\text{outlet}}$	=	outlet bulk temperature, K
T_w	=	average wall temperature, K
V	=	voltage across the heater, V
δ	=	dimple depth
ρ	=	density of air, kg m ⁻³

Introduction

THE importance of heat transfer enhancement has gained greater significance in areas such as microelectronic cooling, macro- and microscale heat exchangers, gas turbine internal airfoil cooling, fuel elements of nuclear power plants, and biomedical devices. A tremendous amount of effort has been devoted to developing new

methods to increase heat transfer from finned surfaces to the surrounding flowing fluid. Rib turbulators, arrays of pin fins, and dimples have been employed for this purpose.

The use of heat sinks is a commonly used solution for thermal management in electronic packaging. Heat sink performance can be evaluated by several factors: material, surface area, flatness of the contact surface, configuration, and fan requirements. Aluminum is commonly used in heat sinks because of its high conductivity (205 W/m°C), low cost, medium weight, and manufacturability. Copper is also used in heat sinks due to its very high thermal conductivity (400 W/m°C), but its disadvantages include high weight and price, as well as fewer choices for production methods. To improve performance, heat sinks should be designed to have a large surface area. In addition, flatness of the contact surface is very important because a nominally flat contact area reduces the interface thermal resistance between the heat sink and source. A heat sink must be designed to allow the cooling fluid to reach all cooling fins and to allow good heat transfer from the heat source to the fins. Heat sink performance also depends on the type of compressor (fan) used because airflow rates have a direct influence on heat transfer.

To obtain higher performance from a heat sink, a large surface, less weight, and lower cost are desired. Thus, efforts to obtain more optimized designs for heat sinks are needed to achieve high thermal performance.

One method to increase the convective heat transfer is to manage the growth of the thermal boundary layer, which can be made thinner or partially broken by flow disturbance. As the boundary layer is reduced by interrupted and/or patterned extended surfaces, convective heat transfer can be increased. Pin fins, protruding ribs, louvered fins, offset-strip fins, slit fins, and vortex generators are typical methods.

Heat transfer augmentation using these methods always results in pressure drop penalties that adversely affect the aerodynamics and overall efficiencies. In the case of cooling of turbine blades, surface protrusions induce excessive pressure losses, thus increasing compressor loads. The separated flowfield over ribs or pin fins can make significant nonuniform cooling, which leads to thermal stresses.

When dimples are placed on the walls of internal flow passages, substantial heat transfer augmentations are observed while pressure drop penalties remain less than those of other types of heat transfer enhancers. Dimples accomplish this by not protruding into the flow region and therefore not generating form drag. Because of easiness of manufacturing, dimples are also attractive as a heat transfer

Received 16 July 2007; revision received 14 November 2007; accepted for publication 21 November 2007. Copyright © 2007 by the American Institute of Aeronautics and Astronautics, Inc. All rights reserved. Copies of this paper may be made for personal or internal use, on condition that the copier pay the \$10.00 per-copy fee to the Copyright Clearance Center, Inc., 222 Rosewood Drive, Danvers, MA 01923; include the code 0887-8722/08 \$10.00 in correspondence with the CCC.

*Graduate Student, Department of Mechanical Engineering, 3123 TAMU.

[†]Texas Engineering Experiment Station (TEES) Associate Research Professor, Department of Mechanical Engineering, 3123 TAMU.

[‡]Texas Engineering Experiment Station (TEES) Research Professor, Department of Mechanical Engineering, 3123 TAMU.

augmentation device; however, there have been few research efforts on the dimple application on heat sinks specifically designed for microelectronic cooling.

Objective

This experimental and numerical investigation was undertaken to provide the needed experimental data and numerical simulations that would partially fill the gap for the use of dimples under a laminar flow regime. Specifically, this investigation was conducted to determine whether or not the use of dimples could enhance heat transfer characteristics for microelectronic heat sink applications. To attain this objective, the following tasks were performed:

1) Experiments with flat and two different kinds of dimpled surfaces.

2) Numerical modeling for flow structure and thermal performance.

Literature Review

Because of dimple's heat transfer enhancement characteristics and lesser pressure penalties, their use for thermal management application has attracted many researchers. One of the earliest research studies on dimples was conducted by Bearman and Harvey [1], who experimentally showed that dimpled circular cylinders can reduce drag force by affecting flow conditions around the circular cylinder similar to dimples on a golf ball. Until now, numerous experimental and numerical studies exist for the use of dimples for turbulent flow, but very little data exist for laminar flow regimes.

The parameters commonly chosen to characterize and evaluate the effects of dimples are the Reynolds number (Re_H), relative channel height (H/D), relative dimple depth (δ/D), and turbulent intensity, and most of the investigations have been conducted for flow in rectangular channels with dimpled walls.

Chyu et al. [2] studied the enhancement of surface heat transfer in a channel with hemispherical and tear-drop-shaped dimples. Concavities serve as vortex generators to promote turbulent mixing in the bulk flow to enhance the heat transfer at $Re_H = 10,000$ to $50,000$, H/D of 0.5, 1.5, 3.0, and $\delta/D = 0.575$. The heat transfer coefficient was 2.5 times higher than that of a smooth channel, with pressure losses that were almost half of those generated by conventional rib turbulators. Moon et al. [3] experimentally studied the effect of channel height on heat transfer performance and friction losses in a rectangular dimpled passage with staggered dimples on one wall. The geometry used was H/D of 0.37, 0.74, 1.11, 1.49, and $Re_H = 12,000$ to $60,000$. Heat transfer enhancement was roughly 2.1 times greater than the smooth channel configuration with H/D values from 0.37 to 1.49. The heat transfer augmentation was invariant with the Reynolds number and channel height. Mahmood et al. [4] studied the flow and heat transfer characteristics over staggered arrays of dimples with $\delta/D = 0.2$ and Reynolds number in the range from 5000 to 35,000. For the globally average Nusselt number, there were small changes with the Reynolds number. Ligrani et al. [5] studied the effect of walls with dimpled protrusions (bumps) on the opposite wall of the dimpled surface.

Mahmood et al. [6] experimentally showed the influence of the dimple aspect ratio, the temperature ratio, Reynolds number, and flow structures in a dimpled channel at $Re_H = 600$ to $11,000$ and the air inlet stagnation temperature ratio of 0.78 to 0.94 with $H/D = 0.20, 0.25, 0.5$, and 1.00 . The results indicated that the vortex pairs which are periodically shed from the dimples become stronger and the local Nusselt number increases as channel height decreases. As the temperature ratio T_{oi}/T_w decreases, the local Nusselt number also increases.

Burgess and Ligrani [7] experimentally analyzed the effect of dimple depth on the surface of a channel with a ratio of dimple depth to dimple printed diameters (δ/D) of 0.1, 0.2, and 0.3. The data showed that the local Nusselt number increased with dimple depth due to an increased strength and intensity of vortices as well as three-dimensional turbulent production, but there was also an increase in friction losses as δ/D increases. Ligrani et al. [8] studied the effect of

the inlet turbulence level in the heat transfer improvement in walls with dimples of ratio $\delta/D = 0.1$ showing that as the turbulence level increased, the relative Nusselt number reduced due to the increased turbulent diffusion of vorticity.

Small et al. [9] experimentally and numerically studied dimpled-wall heat sink performance over a mock microprocessor. A heat sink with a staggered array of nine, eight, and nine rectangular fins with dimpled surfaces showed the best performance—lower temperature—with a total volume 25% less than the value of the baseline heat sink.

Numerical studies in heat transfer improvement over dimpled surfaces have been performed by Lin et al. [10], who presented computational results for a channel with dimpled walls in a turbulent airflow regime. Isaev et al. [11–17] studied the effect of dimple emphasis on the flow structure and heat transfer characteristics in a laminar and a turbulent airflow condition. A relative dimple depth in the range of 0.06 to 0.24 and a SIMPLEC formulation with multiblock grids were used to evaluate flow and heat transfer characteristics over a single dimple on a wall. The effects of Reynolds numbers, both laminar and turbulent, over dimples of $\delta/D = 0.22$, were also studied. The geometry and flow conditions were the same as those used by Chyu et al. [2] to compare with the computed results. This study explained the flow structure and heat transfer enhancement characteristics induced by concavities.

Park et al. [18] numerically examined turbulent airflow in a channel with deep dimples ($\delta/D = 0.3$) using the realizable $k-\epsilon$ model and no wall function for $Re_H = 2700$ to $41,000$. This study provided details of the development of flow structures through the dimples and their subsequent impact on heat transfer. Park and Ligrani [19] studied seven different dimple geometries (spherical, cylindrical, and triangular) presenting relative Nusselt numbers, velocity, and Eddy diffusivity distributions. Spherical and tilted cylindrical dimples showed the best thermal performance.

Silva et al. [20] used Fluent 6.2.16 to numerically investigate heat transfer improvement over dimpled walls under a laminar regime. This study showed relative Nusselt number improvement of 1.65 for a Reynolds number of 500 and dimple pitch of 0.81. Based on the numerical results, Silva rationalized that an increase in dimple pitch would render similar heat transfer enhancement with less friction losses. Dimple pitch was then increased to 1.21, showing a Nusselt number improvement of 1.67 and a friction reduction of 12.6% relative to the original dimple plate.

Silva et al. [21] studied the flow in a channel with dimple surfaces under a laminar regime, both experimentally and numerically. The investigation showed relative Nusselt numbers of 1.10 and 1.06 for oval dimples for laminar flow at Reynolds numbers of 500 and 1000, respectively. The results for a circular dimple were inside the uncertainty values and therefore inconclusive. The dimple geometry and experimental setup used by Silva et al. was the same as in the present work, but included a *separator plate* placed in front of the leading edge of the copper plates to guarantee fully developed hydraulic flow over the dimples. The combined effect of heat transfer improvement and enhanced area of the dimples allowed for an average temperature reduction of 3.7 K in the dimple plate when compared to the flat plate with the same dimensions.

Experimental Detail

Experimental Setup

A schematic drawing of the facility used for heat transfer measurements is shown in Fig. 1. The experimental setup consists of an open loop flow circuit with a test section, a rectangular channel, a plenum, a calibrated orifice flow meter, a gate valve, and a centrifugal blower. The inner channel cross-section dimensions are 32 mm (width) and 103.5 mm (height). The channel was constructed with 8.3-mm-thick acrylic plates with thermal conductivity $k = 0.16$ W/m °C at 20°C and the channel included a 2500-mm-long entrance section. A $300 \times 300 \times 450$ mm plenum fabricated with wood panels was used to stabilize the flow drawn by the blower.

Figure 2 shows the cross section of the test section. All exterior surfaces of the test section are insulated with fiberglass

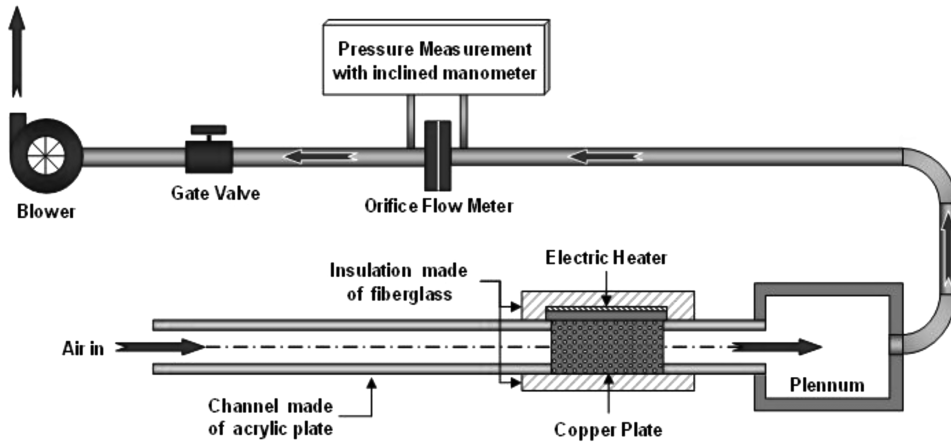


Fig. 1 Schematic drawing of the test equipment.

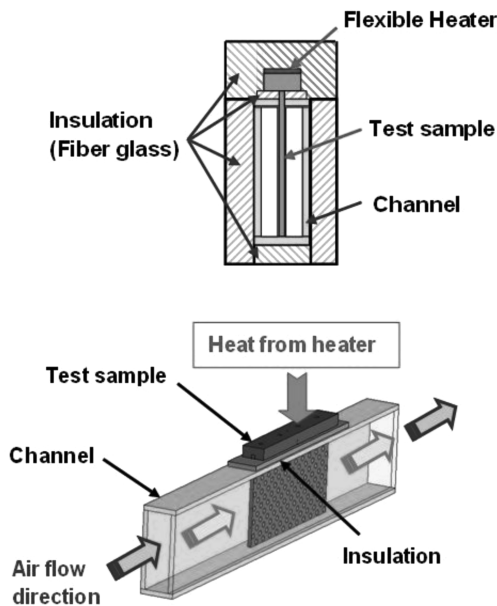


Fig. 2 Test section.

($k = 0.04 \text{ W/m}^\circ\text{C}$) to minimize heat losses. An Omega electric heater model KH-108/5-P (Kapton, $25.4 \times 203.2 \text{ mm}$, 115 V , 40 W total power, pressure sensitive adhesive on one side) was used to provide a constant heat flux to the copper plate. The heaters allowed a heat flux up to 40 kW/m^2 through the 5-mm -thick test plate. Power to the heater was controlled by an Elenco-Precision variable power supply model XP-800, with multimeter TENMA models 72-6685A and 72-6185 used to measure voltage and current into the heater.

Figure 3 shows the CPU and heat sink with dimples. Only one fin was used to study the heat transfer enhancement characteristics. In published literature the heat flux is commonly applied from the bottom of the plate, as shown in Fig. 4a. In this investigation, heat flux was applied from the top of the plate, as shown in Fig. 4b, to simulate an actual heat sink application in the laboratory environment.

Figures 5a–5c present the geometric details of the test surface including dimple geometry. Figure 5b shows the circular dimpled plate with 11×22 dimples while Fig. 5c shows the oval dimpled plate with 7×22 dimples on each side. The circular dimples were placed on both sides of the copper plate with relative pitch $S/D = 1.21 \text{ m}$, with S being the dimple center to center in the direction of the flow, and a relative depth δ/D of 0.2 . Relative channel height H/D was 1.86 . For the oval dimples, S/D was 1.21 and δ/D was 0.2 with the same total depth and circular edge-to-edge distance as the circular dimples. The oval dimples used in this

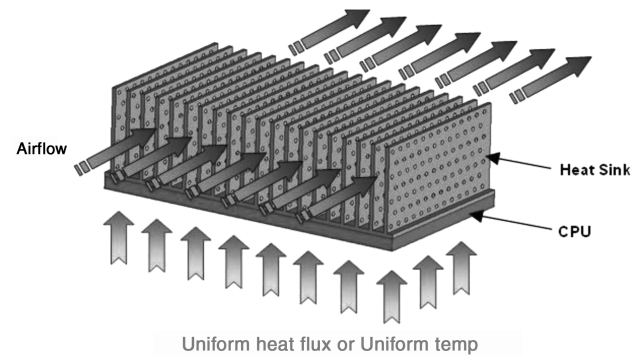
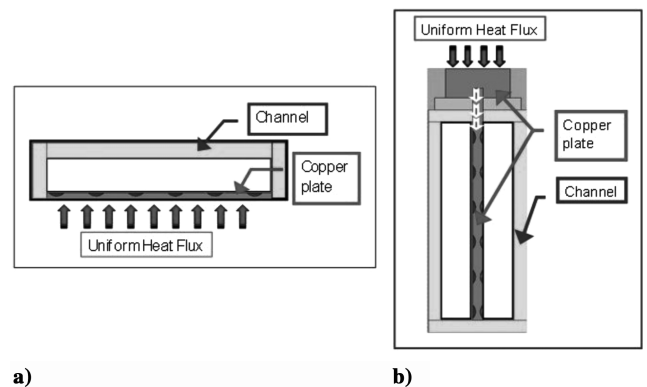


Fig. 3 CPU and heat sink with circular dimples.



a) b)
Fig. 4 Test section of a) a general square channel, and b) present experimental channel.

investigation have been previously referenced by Isaev et al. [17] as *trenched* dimples as they consist of two spherical halves with a cylindrical insert. The length of the insert in our oval dimples was 75.8% of the dimple diameter and the axis of the insert was aligned 90° deg with respect to the flow direction.

Three test plates were fabricated with 5-mm thickness ASTM-B152 electroless, oxygen-free copper. The temperature of the test plate was measured using nine calibrated copper-constantan thermocouples, shown in Fig. 6. A flat projected area was used to calculate the heat transfer coefficient and a Nusselt number.

Uncertainty Analysis

The uncertainty of the average heat transfer coefficient depends on the uncertainties in the average wall temperature, bulk air temperature difference, and the net heat input for each test section. This uncertainty increases with decreasing both the average wall

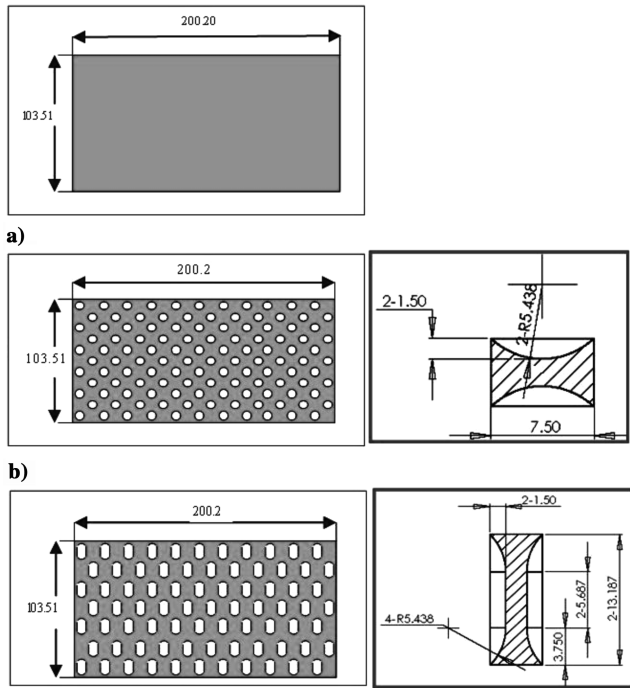


Fig. 5 Schematic drawings: a) the entire test surface of the flat copper plate; b) plate with circular dimple dimensions; c) plate with elliptical dimple dimensions. All dimensions are given in mm.

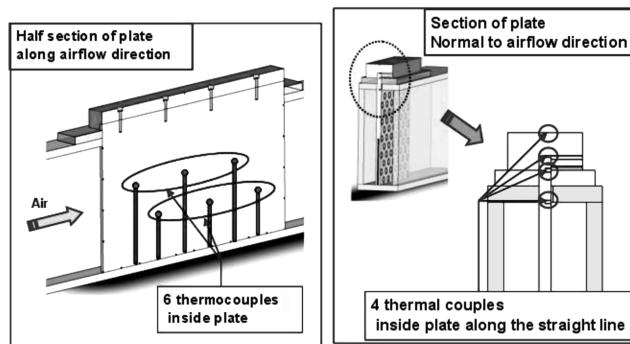


Fig. 6 Thermocouple location.

temperature to bulk air temperature difference and the net heat flux. Based on a confidence level of 95% described by Kline and McClintock [22], uncertainty values of $\pm 0.5\%$ for all properties of the air, and $\pm 0.5\%$ for all physical dimensions were used.

Based on the maximum uncertainties for pressure at the orifice flow meter, and the pressure drop across the orifices of ± 1.0 and $\pm 4.1\%$, respectively, the maximum uncertainty of the air mass flow rate was calculated to be $\pm 2.8\%$. The corresponding maximum uncertainty of the Reynolds number was ± 2.9 . The uncertainties for the power input and heat loss were found to be ± 3.1 and $\pm 5.4\%$, respectively, and those for the average wall and bulk temperatures ± 3.0 and $\pm 3.5\%$, respectively. With these values, the uncertainty of the Nusselt number was calculated to be $\pm 7.8\%$.

Numerical Detail

Computational Grid

Numerical studies were conducted to determine the heat transfer and velocity profiles on a rectangular channel, replicating the flow inside the *gap* formed between two fins of a heat sink as shown in Fig. 3. The numerical domain consisted of half-thickness of a dimpled plate plus half-height of a gap. Looking at Fig. 4b, the domain covered from the centerline of the middle plate (copper) to

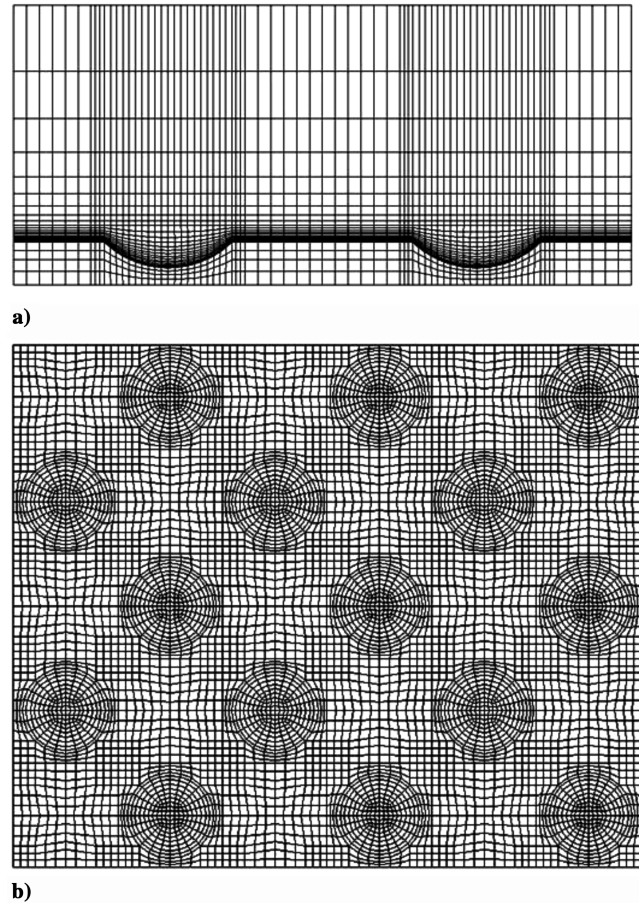


Fig. 7 The side and top views of the circular dimple plate.

the centerline of one of the channels, with the flow coming perpendicularly to the plane of the figure. This selection was made to take advantage of symmetry boundary conditions at the center planes of the copper plate and the channel. Previous studies [3,6] reported that when channel height is $2\times$ or higher than dimple depth (our is $4.6\times$), the effect of the opposite wall on the heat transfer in the dimpled wall is negligible and therefore, a symmetry boundary condition can be used in this plane to model several fins. Periodic boundary conditions were not used along the flow axis due to the heat flux direction, which instead of coming from the back of the plate, was coming from the side, as shown in Fig. 4.

Figures 7 and 8 show side and top views of sections of the computational grid used for the circular dimples and oval dimples. Hexahedral elements aligned with the flow direction were used to reduce the numerical dissipation errors and improve the quality of numerical predictions. Fine grids were employed for near-wall and dimpled surfaces to resolve the high gradients encountered in these regions. The numbers of finite volume hexahedral cells employed for the entire flow domain and each region are shown in Table 1. Computational models included all the dimples shown in Fig. 5.

Boundary conditions were specified as symmetry boundaries in the top and bottom of Fig. 7a (half-planes of the copper plate and channel), insulated walls on the sides of the channel, free outflow at the channel exit, and velocity inlet with air at 300 K at the channel inlet. Air velocity was calculated based on the total channel height and the desired Reynolds number.

Computational Model

The SIMPLE (semi-implicit method for pressure-linked equations) algorithm, along with a structured grid, was used to couple the pressure and velocity fields. The second-order upwind interpolation scheme and spatial discretization were used to reduce numerical errors.

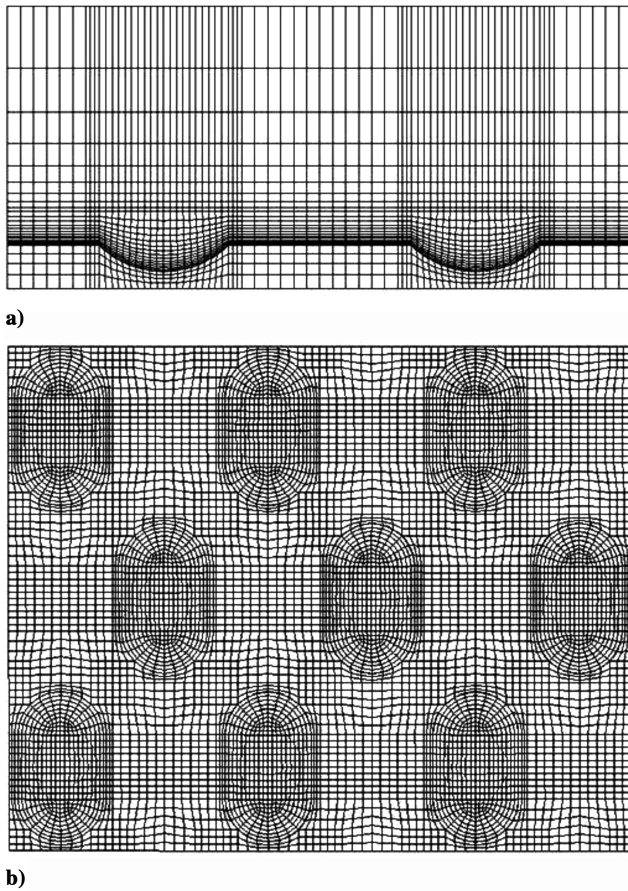


Fig. 8 The side and top views of the oval dimple plate.

Grid Independence and Solution Convergence

Three different sets of grids were tested for grid independence of the circular and elliptical dimpled plates: 6×8 , 8×13 , and 10×16 , depending on the number of elements inside the dimples.

Table 2 shows the three different sets of grids tested for grid independence. A 6×8 type means six divisions on the edge of one-quarter of a dimple and eight divisions in the line form this edge to the center, following the surface, for a total of 48 surface elements on one quarter-dimple. 8×13 and 10×16 types follow a similar grid scheme.

It was found that heat transfer prediction varied less than 2% with these grid selections and therefore the 6×8 type was used. The implicit method was employed to the computational iteration. Scaled residuals were used for the convergence of the computational solutions for the continuity, energy, and for the other predicted variables. The setting criterion of the scaled residuals for the solution convergence was 1×10^{-3} for all computed residuals except for the energy equation 1×10^{-6} .

Results and Discussion

Experiment Results

Experiments were conducted to obtain the Nusselt number improvement in a heat sink with dimpled surfaces relative to a unit with flat surfaces. Three copper plates with different surface characteristics were fabricated and used to obtain the average heat

transfer coefficient. Dimples were placed on both sides of two copper plates. Each plate was placed in the middle of the rectangular channel and a uniform heat flux was applied in the in-plane axis of the plate. The flat plate was used as baseline data. Average heat transfer coefficients were calculated for four different Reynolds numbers based on channel height (Re_H) from 500 to 1650 and a uniform heat flux of 14 kW/m^2 .

Figure 9 shows the convection heat transfer coefficients for three different plates. These coefficients were calculated using the average temperature of each copper plate from the thermocouples and the average of the inlet and outlet air temperatures, with the total heat transferred to the air calculated by energy balance between inlet and outlet flows. The area used for calculations was the flat projected area of each plate. Results showed that heat transfer coefficients increased with increasing airflow and that for all airflow velocities, heat transfer coefficients for the circular and oval dimple plates were higher than those of the flat plate.

In Fig. 10 the Nusselt numbers of the circular and oval plates relative to the flat plate are presented. Nusselt numbers were calculated based on the convective coefficients previously obtained, the conductivity of the air at the average temperature, and the channel height. At very low flow velocity ($Re_H = 500$), Nu/Nu_0 values for circular and oval type dimpled plates were less than 1.02. For Re_H from 750 to 1650, Nu/Nu_0 values for both circular and oval dimples were around 1.06, regardless of Re_H .

Numerical Results

The same geometries and similar test conditions as in the experimental setup were used to simulate the heat transfer coefficient, pressure drop, thermal performance, and flow patterns using FLUENT 6.2.16.

Figure 11 shows the heat transfer coefficients comparison of the experimental and numerical models for the four different Reynolds numbers of 500, 750, 1000, and 1650. The results of the numerical simulations showed the same trend as the experimental data; however, the heat transfer coefficients of the numerical results were smaller than the experimental results. The lower heat transfer coefficients in the numerical simulation are probably due to mixing effects. In the experiments, even though flow was laminar, some degree of turbulence was generated over the first section of the channel, just after the flow impinging over the leading edge of the plate. The numerical simulation was run under the laminar viscosity model and failed to capture any turbulence generated, therefore giving lower overall Nusselt numbers. This effect would increase in the upper range of the Reynolds number studied (over 1500). Moreover, neither heat losses nor natural convection effects were considered in the numerical simulation. With a temperature difference of 20°C between the dimple plate and the incoming air, the natural-convection-only coefficient for the experiment conditions was estimated in $5.2 \text{ W/m}^2 \cdot ^\circ\text{C}$. This value would shift the lines in Fig. 11 toward the experimental results and partially explain the differences. Nevertheless, relative Nusselt numbers Nu/Nu_0 showed similar values in both numerical and experimental studies.

Figure 12 shows the friction factor ratio f/f_0 for circular and oval dimple plates for Reynolds numbers of 500, 750, 1000, and 1650. The pressure drops of the dimpled plates for laminar airflow were either equivalent to or less than values produced in the flat plate with no dimples. In the case of the circular dimples the friction factor ratio was roughly 0.94. The friction factor ratio for the oval dimples was

Table 2 Sets of grids used for grid independence check

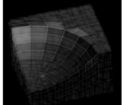
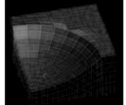
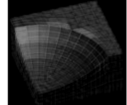
	6×8 type	8×13 type	10×16 type
Shape			
Plate element no.	1,219,488	1,995,296	2,607,776

Table 1 Number of finite volume cells for each domain

Plate	Inlet region	Plate region	Outlet region	Total
Flat	99,000	672,000	99,000	870,000
Circular	182,250	1,511,136	182,250	1,875,636
Oval	207,900	1,738,044	207,900	2,153,844

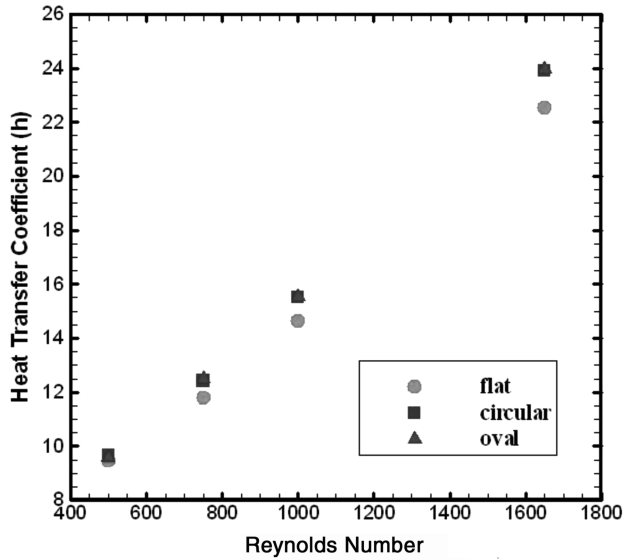


Fig. 9 Heat transfer coefficient in $W/m^2 \cdot ^\circ C$ for the test plates.

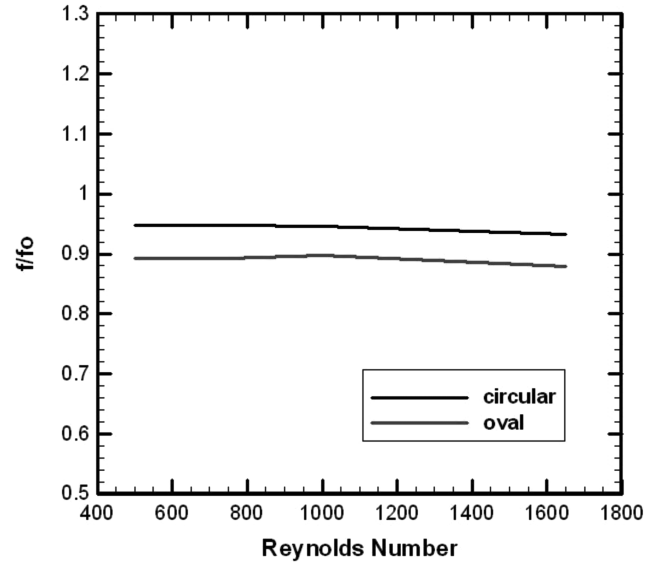


Fig. 12 Relative friction factor ratio for the dimple plates.

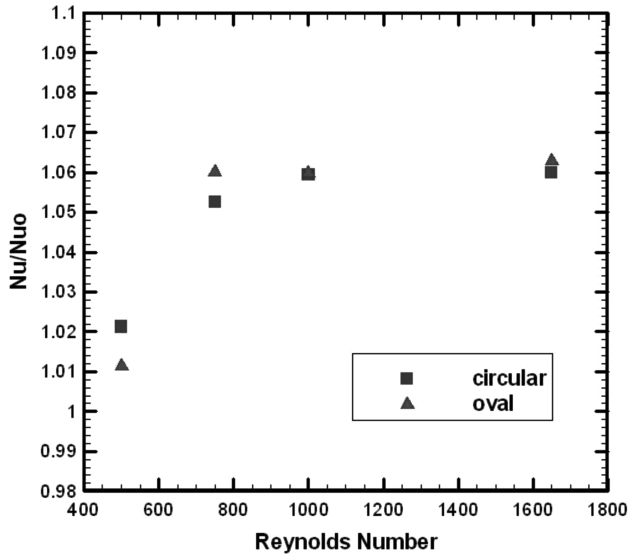


Fig. 10 Relative Nusselt number for the dimple plates.

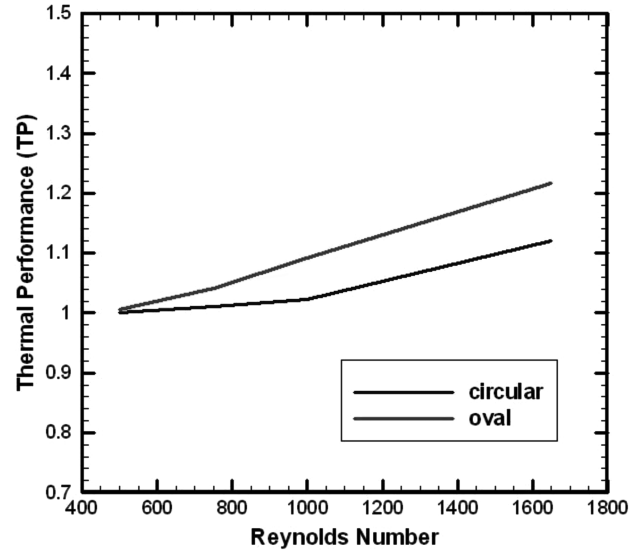


Fig. 13 Thermal performance for the dimple plates.

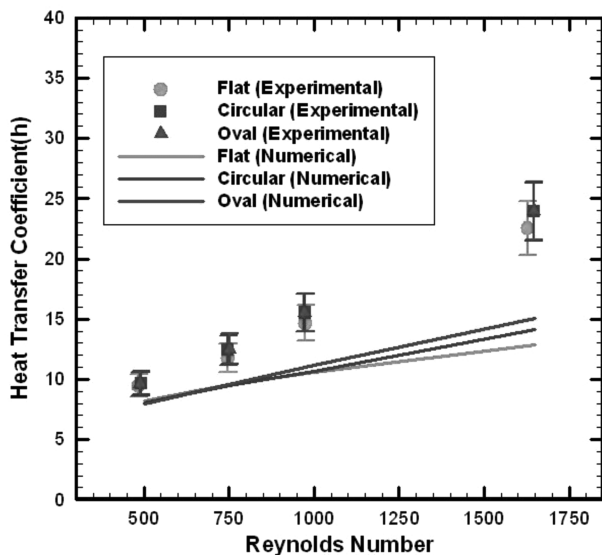


Fig. 11 Heat transfer coefficient in $W/m^2 \cdot ^\circ C$ for the test plates.

0.89. The average pressure drop for the oval dimples was smaller than that of the circular dimples over all the Reynolds number range. This was expected given that there are less oval dimples than circular ones over a given fixed area.

The thermal performance factor was evaluated with Eq. (1) using the average Nusselt number and friction factor relative ratios. This parameter compares the heat transfer enhancement by the dimples per unit pumping power relative to the heat transfer for the flat plate,

$$TP = (Nu/Nu_0)(f/f_0)^{-1/3} \quad (1)$$

Figure 13 compares the thermal performance factor for two different dimple plates tested. Both cases showed that the thermal performance factor increases with increasing mass flow rate. The thermal performance factor for the oval dimple plate increased from 1.0 to 1.21, while for the circular dimple plate the value increased from 1.0 to 1.12. In general, oval dimples showed better performance than circular dimples for all cases tested.

The flow structure was briefly investigated by analyzing the numerical model. The streamwise sectional view, spanwise sectional view, top view over a dimple, and top view inside a dimple were plotted to visualize the flow structure.

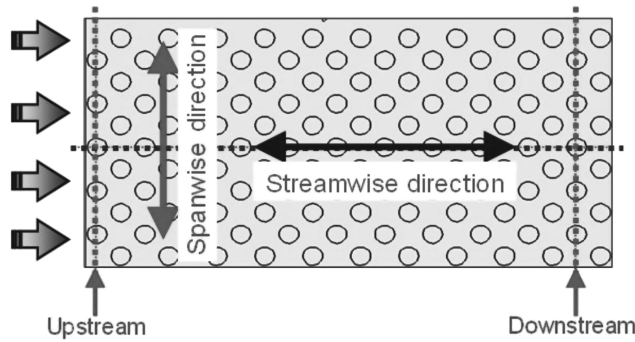
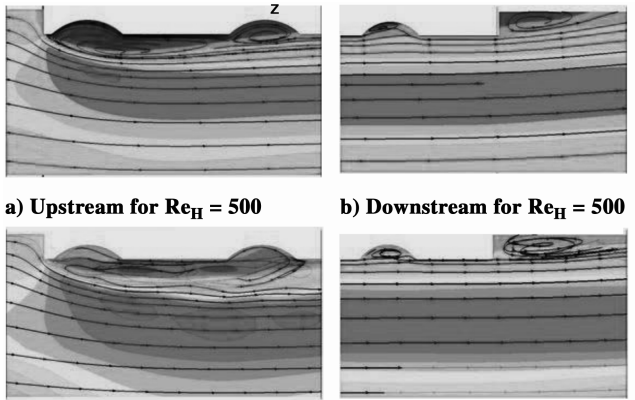
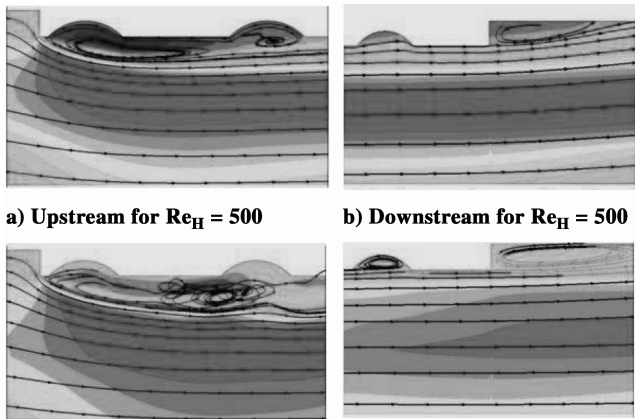


Fig. 14 Schematic diagram of planes used to compute the streamwise development over dimples.



c) Upstream for $Re_H = 1650$ d) Downstream for $Re_H = 1650$
Fig. 15 Streamline of upstream and downstream for the circular dimple.



c) Upstream for $Re_H = 1650$ d) Downstream for $Re_H = 1650$
Fig. 16 Streamline of upstream and downstream for the oval dimple plate.

Figure 14 shows the schematic diagram for a circular dimple plate with the reference locations for the discussion and plots that follows. Figures 15 and 16 show streamwise section views of the circular and oval dimpled plates for $Re_H = 500$ and $Re_H = 1650$, respectively. Stronger and larger recirculation regions exist for both the upstream and downstream regions at $Re_H = 1650$. The vortices inside of the dimples are shown at the downstream region for both the circular and oval dimpled plates. Reattachment is evident at the landing area trailing the dimples. This flow reattachment enhances the local convection heat transfer coefficient; but on the other hand, a recirculation zone reduces heat convection because the flow is trapped in that zone.

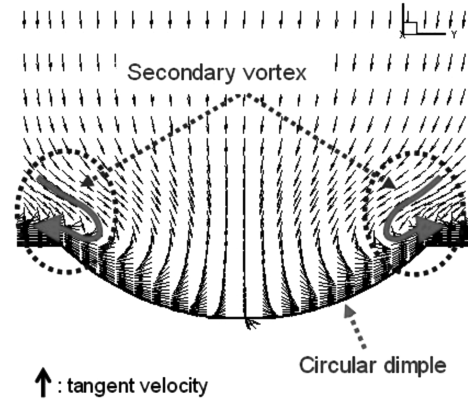


Fig. 17 Downstream spanwise sectional view for the circular dimple plate.

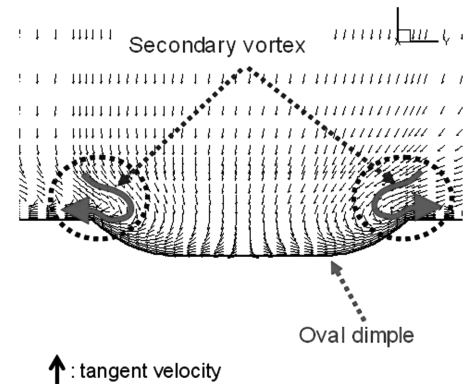


Fig. 18 Downstream spanwise sectional view for the oval dimple plate.

Figures 17 and 18 show downstream, spanwise, sectional views of the circular and oval dimple plates, respectively. In these figures the secondary vortices are evident around the spanwise corner of both circular and oval dimples. These secondary vortices also enhance the local convection heat transfer due to the reattachment.

Figure 19 shows the top view inside of the circular and oval dimples for $Re_H = 500$ and $Re_H = 1650$ at the downstream region. A higher intensity recirculation is shown for $Re_H = 1650$ compared to $Re_H = 500$. In the case of the oval dimple, the larger recirculation inside of the dimple enhances the flow mixing leading to increased heat transfer.

The numerical results showed, in general, the same phenomena observed in the experimental results of this investigations and previously published literature. Dimples generate self-organized vortices into and downstream of the cavity (dimple) itself, drawing cold fluid from the freestream to the area near the wall and therefore improving the overall heat transfer. At the lower Reynolds number tested ($Re_H = 500$) there is basically no vortices nor recirculation and thermal improvement for the dimple plate is minimum, more likely due to area enhancement. As Reynolds numbers increase, the vortices become stronger and the heat transfer coefficient improves.

The numerical simulation also showed, as in previous investigations, that the area around and behind the trailing edge of the dimples has the best heat transfer coefficient, and that optimization of such area will render better overall performance. The oval dimple studied in this investigation has a larger dimple-trailing edge area to number-of-dimples ratio and both experimental and numerical data showed oval dimples had better heat transfer and lower friction coefficients.

Conclusions

This investigation presents experimental and numerical results for the heat transfer characteristics of a heat sink for laminar airflow conditions using two different types of dimples in a plate. The

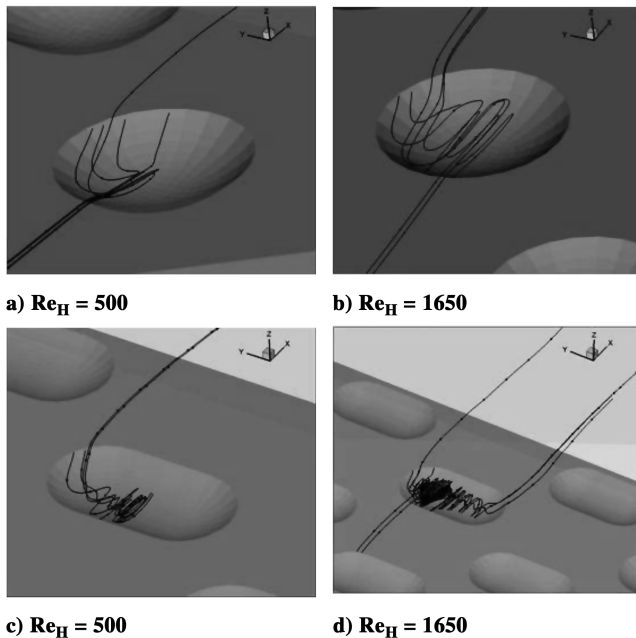


Fig. 19 Streamwise top view inside of the dimples.

average heat transfer and heat transfer enhancement were obtained experimentally. Heat transfer, pressure drop, thermal performance, and flow conditions were numerically simulated.

Experiments using heated copper plates in a rectangular channel under laminar flow were performed to obtain heat transfer characteristics for a heat sink with dimpled surfaces. Three copper plates with different surface patterns, flat, circular dimples, and oval dimples, were fabricated and used to obtain the average heat transfer. Dimples were placed on both sides of each copper plate, and then the plates were located in the middle of the rectangular channel where a uniform heat flux was applied in the in-plane axis of the plate. The flat plate was used for baseline data. The findings of this experimental study are summarized as follows:

1) Heat transfer coefficient for the test plates increased with increasing mass flow rate, for example, Reynolds number.
2) At low Reynolds number ($Re_H = 500$), the relative Nusselt number ratio Nu/Nu_0 for circular and oval dimple plates was less than 1.02.

3) For Reynolds number from 750 to 1500, Nu/Nu_0 ratios for both circular and oval cases were approximately 1.06 regardless of Re_H . This value was consistent, but inside the uncertainty margins.

The same geometries and test conditions with the experimental study were used to simulate heat transfer coefficient, pressure drop, thermal performance, and flow by using FLUENT version 6.2.16. The findings of this numerical study are summarized as follows:

1) The relative heat transfer coefficients of the numerical results are very similar to those of the experimental results, but the absolute heat transfer coefficients of the numerical results were smaller than those of the experiments.

2) The pressure drops over the dimple plates in the laminar regime were either equivalent to or less than values produced in a flat plate with no dimples. The pressure drop of the oval dimple plate was smaller than that of the circular dimple plate.

3) As the Reynolds number increased, the thermal performances of both circular and oval dimple plates increased. Generally, the thermal performance of the oval dimples was higher than that of the circular dimples.

4) Both the circular and oval dimple plate simulations showed that a prime vortex pair results from the recirculation region inside of the dimples. Primary vortices are positioned in the upstream of the dimple. As the airflow increased, the primary vortices were also extended in the downstream direction and grew larger and stronger. The oval dimple plate had larger primary vortices than the circular plate for the same airflow condition.

5) Secondary vortex flows are observed at each side of the dimples. The reattachment of the central and secondary vortex flows occurred at the trailing edge region of the dimples, increasing the heat transfer coefficient in this area.

From the experimental and numerical studies, it can be concluded that heat transfer enhancement was observed in the dimpled surfaces tested. Dimples enhanced heat transfer while keeping the pressure losses to a minimum. These surfaces do indeed enhance thermal performance without the penalty of higher pressure drops typical of flow-protruding turbulence promoters. Through these observations, dimple surfaces show the potential to be employed in heat sink applications for microelectronic cooling under laminar flow.

References

- [1] Bearman, P. W., and Harvey, J. K., "Control of Circular Cylinder Flow by the Use of Dimples," *AIAA Journal*, Vol. 31, 1993, pp. 1753–1756.
- [2] Chyu, M. K., Yu, Y., Ding, H., Downs, J. P., and Soechting, F. O., "Concavity Enhanced Heat Transfer in an Internal Cooling Passage," ASME, Paper 97-GT-437, 1997.
- [3] Moon, H. K., O'Connell, T., and Glezer, B., "Channel Height Effect on Heat Transfer and Friction in a Dimpled Passage," ASME Paper 99-GT-163, 1999, p. 307.
- [4] Mahmood, G. I., Hill, M. L., Nelson, D. L., Ligrani, P. M., Moon, H. K., and Glezer, B., "Local Heat Transfer and Flow Structure on and Above a Dimpled Surface in a Channel," *Journal of Turbomachinery*, Vol. 123, Jan. 2001, pp. 115–123. doi:10.1115/1.1333694
- [5] Ligrani, P. M., Mahmood, G. I., and Sabbagh, M. Z., "Heat Transfer in a Channel with Dimples and Protrusion on Opposite Walls," *Journal of Thermophysics and Heat Transfer*, Vol. 15, No. 3, 2001, pp. 275–283.
- [6] Mahmood, G. I., and Ligrani, P. M., "Heat Transfer in a Dimpled Channel: Combined Influences of Aspect Ratio, Temperature Ratio, Reynolds Number, and Flow Structure," *International Journal of Heat and Mass Transfer*, Vol. 45, 2002, pp. 2011–2020. doi:10.1016/S0017-9310(01)00314-3
- [7] Burgess, N. K., and Ligrani, P. M., "Effects of Dimple Depth on Channel Nusselt Numbers and Friction Factors," *Journal of Heat Transfer*, Vol. 127, No. 8, 2005, pp. 839–847. doi:10.1115/1.1994880
- [8] Ligrani, P. M., Burgess, N. K., and Won, S. Y., "Nusselt Numbers and Flow Structure on and Above a Shallow Dimpled Surface Within a Channel Including Effects of Inlet Turbulence Intensity Level," *Journal of Turbomachinery*, Vol. 127, 2005, pp. 321–330. doi:10.1115/1.1861913
- [9] Small, E., Sadeghipour, S. M., and Asheghi, M., "Heat Sinks with Enhanced Heat Transfer Capability for Electronic Cooling Applications," *Journal of Electronic Packaging*, Vol. 127, April 2005, pp. 285–290.
- [10] Lin, Y. L., Shih, T. I., and Chyu, M. K., "Computations for Flow and Heat Transfer in a Channel with Rows of Hemispherical Cavities," ASME Paper 99-GT-263, 1999.
- [11] Isaev, S. A., Leontiev, A. I., Usachev, A. E., and Frolov, D. P., "Numerical Simulation of Laminar Incompressible Three-Dimensional Flow Around a Dimple (Vortex Dynamics and Heat Transfer)," *Russian Ministry of Science and Technology Institute for High-Performance Computing and Databases*, 1997, pp. 6–67 (preprint).
- [12] Isaev, S. A., Leontiev, A. I., Metov, K. T., and Kharchenko, V. B., "Modeling of the Influence of Viscosity on the Tornado Heat Exchange in Turbulent Flow Around a Small Hole on the Plane," *Journal of Engineering Physics and Thermophysics*, Vol. 75, No. 4, 2002, pp. 890–898. doi:10.1023/A:1020315118820
- [13] Isaev, S. A., Leontiev, A. I., Metov, K. T., and Kharchenko, V. B., "Verification of the Multiblock Computational Technology in Calculating Laminar and Turbulent Flow Around a Spherical Hole on a Channel Wall," *Journal of Engineering Physics and Thermophysics*, Vol. 75, No. 5, 2002, pp. 1155–1158. doi:10.1023/A:1021123909988
- [14] Isaev, S. A., and Leontiev, A. I., "Numerical Simulation of Vortex Enhancement of Heat Transfer Under Conditions of Turbulent Flow Past a Spherical Dimple on the Wall of a Narrow Channel," *High Temperature*, Vol. 41, No. 5, 2003, pp. 665–679. doi:10.1023/A:1026100913269
- [15] Isaev, S. A., Leontiev, A. I., Baranov, P. A., Metov, K. T., and Usachev, A. E., "Numerical Analysis of the Effect of Viscosity on the Vortex Dynamics in Laminar Separated Flow Past a Dimple on a Plane with

- Allowance for its Asymmetry," *Journal of Engineering Physics and Thermophysics*, Vol. 74, No. 2, 2001, pp. 339–346.
doi:10.1023/A:1016600404896
- [16] Isaev, S. A., Leontiev, A. I., and Baranov, P. A., "Identification of Self-Organized Vortex-Like Structures in Numerically Simulated Turbulent Flow of a Viscous Incompressible Liquid Streaming Around a Well on a Plane," *Technical Physics Letters*, Vol. 26, No. 1, 2000, pp. 15–18.
doi:10.1134/1.1262724
- [17] Isaev, S. A., Leontiev, A. I., and Kudryavtsev, N. A., "Numerical Simulation of Hydrodynamics and Heat Transfer Under Conditions of Turbulent Transverse Flow Past a "Trench" on a Plane Surface," *High Temperature*, Vol. 43, No. 1, 2005, pp. 086–099.
- [18] Park, J., Desam, P. R., and Ligrani, P. M., "Numerical Predictions of Flow Structures Above a Dimpled Surface in a Channel," *Numerical Heat Transfer*, Vol. 45, 2004, pp. 1–20.
doi:10.1080/1040778049026740
- [19] Park, J., and Ligrani, P. M., "Numerical Predictions of Heat Transfer and Fluid Flow Characteristics for Seven Different Dimpled Surfaces in a Channel," *Numerical Heat Transfer*, Vol. 47, 2005, pp. 209–232.
doi:10.1080/10407780590886304
- [20] Silva, C., Marotta, E., and Fletcher, L., "Flow Structure and Enhanced Heat Transfer in Channel Flow with Dimpled Surfaces: Application to Heat Sinks in Microelectronic Cooling," *Journal of Electronic Packaging*, Vol. 129, June 2007, pp. 157–166.
doi:10.1115/1.2721087
- [21] Silva, C., Park, D., Marotta, E., and Fletcher, L., "Optimization of Heat Sink Performance in Microelectronics Through Dimpled Surfaces: Study on Dimple Geometry and Array," *Proceedings of the 2007 ASME Graduate Student Research Innovation Conference*, ASME, Fairfield, NJ, April 2007.
- [22] Kline, S. J., and McClintock, F. A., "Describing Uncertainties in Single Sample Experiments," *Mechanical Engineering*, American Society of Mechanical Engineering, Vol. 75, No. 1, 1953, pp. 3–8.